Metallurgical and Materials Engineering *Research paper*
Association of Metallurgical Engineers of Serbia AMES *https://doi.org/10.30544/832*

DEFORMATION BEHAVIOR AND PROCESSING MAP OF ATI 425 WITH INITIAL LAMELLAR MICROSTRUCTURE

R. Mahdavi[1], E. Emadoddin[1], S. M. Abbasi[2]*

[1]*Faculty of Materials and Metallurgical Engineering, Semnan Univesity, Semnan, Iran*
[2]*Faculty of Materials and Manufacturing Technologies, Tehran, Iran*

Received 25.04.2022
Accepted 20.06.2022

Abstract

The effect of hot compression temperatures and strain rates on deformation behavior and resultant microstructure of ATI 425 alloy with initial lamellar microstructure was investigated in this study. The temperature and strain rate of the hot compression test were chosen to be in the 700-1100 °C and 0.001-1 s^{-1} ranges, respectively. The stress-strain curve and microstructure evaluation show that the alloy's flow softening is associated with globularization and dynamic recrystallization mechanisms. The constitutive equation calculates the activation energy for the α/β and β regions to be 348 kJ/mol and 201 kJ/mol, respectively. Dynamic recovery and partial recrystallization are the dominant structure modification mechanisms in the beta single-phase region. Bending and fragmentation of alpha plates is the dominant mechanism of microstructure promotion in the α/β region at low temperatures and low strain rates, less than $0.1s^{-1}$. Local shear and alpha plate break-up are the main factors in structural modification at high strain rates, greater than $0.1s^{-1}$. The extracted process map at 0.5 strain revealed three zones: instability, safe zone, and peak zone, with power dissipation efficiencies of 0 -0.25%, 30-40%, and above 40%.

Keywords: ATI425 alloy; lamellar microstructure; dynamic recrystallization; bending and fragmentation; processing map.

[*] Corresponding author: E. Emadoddin, *emadoddin@semnan.ac.ir*

Introduction

ATI425 alloy is a new α/β titanium alloy with comparable mechanical properties at room temperature and a lower production cost when compared to other titanium alloys, particularly Ti6Al4V. Furthermore, this alloy has a high potential for use in aerospace [1]. ATI 425 alloy's mechanical properties are directly related to its initial microstructure and crystallographic texture. The hot deformation process has been extensively studied for microstructure modification.

The following are two critical factors that have a significant impact on microstructure development: 1) alpha and beta phase initial morphology, and 2) deformation parameters Applied strain, strain rate, and deformation temperature have also been identified as important deformation parameters [2]. *Margolin and Cohen* [3] stated that recrystallized -grains are a major source of lamellar fragmentation. As a result, the driving force of surface tension has caused the migration of alpha/beta boundaries. It was also shown that dynamic spheroidization of lamellar microstructures (with medium layer thickness) occurred at relatively low strains via cross slip and glide/climb [4, 5]. According to *Weiss'* research [6] the promoted shear bands through the palate of the lamellar alpha phase are attributed to dynamic spheroidization. As a result, the evolution of high-energy alpha/alpha interfaces in contact with beta plates resulted in alpha phases penetrating. *Park et al.* [7] proposed three steps for alpha lamellar dynamic spheroidization. Layer bending occurs during the first stage. Second, along the shear bands, both signs of dislocations have been generated. The glide or climb process then causes annihilation of opposite sign dislocations, and a few globules are pushed by surface migration to reduce interfacial energy.

The mechanism in the β single-phase zone differs from that in the two-phase zone. Dynamic recovery (DRV) is an important deformation softening mechanism in the region. *Wang et al.* [8] discovered that the mechanism of microstructural mechanical transformation in the Ti53311S beta titanium alloy is dynamic recovery. *Han et al.* [9] also confirmed the dynamic recovery in beta grains during beta range work in the Ti600 alloy. The primary beta grains are elongated on a plane perpendicular to the axial compression direction, resulting in the three-dimensional structure produced by a high DRV in the working beta range. Recrystallization of beta grains is frequently observed in the primary of the beta grain boundary, where DRX nuclei begin. This phenomenon results in the formation of a visible necklace of fine coaxial beta beads stretched and deformed around the initial beta phase [10].

The temperature of deformation also has a significant impact on the evolution of the microstructure in the beta region. DRX has been observed to occur with difficulty in the phase range at low temperatures. The amount of DRX, on the other hand, increases with temperature. *Ding et al.* [11] found that increasing the temperature from 1000 to 1050 increased recrystallization by 30% on Ti-6Al-4V titanium alloy.

The microstructure evolution influenced by the strain during the hot working in the β range. DRX grains is not visible until the strain reaches a certain threshold. With strain, the DRX grain fraction expands rapidly. According to *Wanjara et al.* [12], the value fraction of DRX is significantly related to the applied strain. The obtained results show that increasing the applied strain from 0.2 to 1.2 significantly increases the volume fraction of DRX from 2.3% to 50%. Throughout the test, the strain rate and deformation temperature remained constant at 1 and 1050 °C, respectively. A processing map is a useful tool for defining the material's response to high temperature deformation. The

stable and unstable deformation zones can be distinguished using the process map. Furthermore, the promoted microstructure in the vicinity of stable deformation has been predicted based on maximum power dissipation efficiency. In addition, the working conditions of the investigated alloy have been optimized. As a result, the defects caused by hot working have been inhibited, and free defected parts have been acquired during the deformation process.

The main aim of this paper is to investigate the effect of deformation parameters on the dynamic globularization process. Therefore, firstly, the lamellar microstructure was developed via thermo-mechanical route. Subsequently, the flow curve and processing map were derived in the studied alloy by manipulating the hot compression test data. Also, according to the microstructure examination, the volume fraction and mechanism of dynamic spheroidization was investigated. Consequently, the compression behavior was optimized based on obtained results. initial lamellar microstructure

Experiment

The initial briquettes were compacted according to the nominal composition of the studied alloy. Then, after welding the compacted briquettes, the primary electrodes were manufactured. During the welding process, the CP-titanium has been used as a filler metal. For increasing the cleanness of the produced electrodes. They were remelted in a vacuum arc remelting (VAR) furnace 2 times. The capacity of the VAR furnace was 20 Kg and its vacuum level was in the range of 10-3. Finally, the manufactured ingot with a height of 150 mm and diameter of 90 mm was obtained. The chemical composition of the provided ingot has been characterized by optical emission spectroscopy (OES) using BELEC device. The content of the hydrogen, oxygen, and nitrogen has been determined by Leco-Tech machine. the result of chemical analysis has been characterized as per following (wt. %): C = 0.01, Al= 3.75, V = 2.53, Fe = 1.76, O= 0.24, H = 0.0029, N = 0.01. So, the chemical composition of the studied alloy is in accordance with AMS 6946. Subsequently, the transus temperature (Tβ) of the studied alloy has been measured via immediate annealing and quenching technique. Based on microstructure evaluation, the transus temperature has been approximately detected to be 945 ± 5°C. The thermomechanical route of the studied alloy has been schematically illustrated in figure 1. As can be seen, the thermomechanical route has been divided into four stages as per following: 1) homogenization at 1150°C, 2) primary hot rolling at 1100°C, 3) secondary hot rolling at 900°C, and finally 4) annealing at 1100°C. The resultant microstructure of this thermomechanical route is fully lamellar.

After achieving the desired microstructure, the effect of hot compression parameters on the alloy's deformation response was studied. The hot compression test was performed in accordance with ASTM E9 for this purpose. The strain rate and deformation temperature were in the 700-1000°C and 0.001-1 s^{-1} ranges, respectively. The Instron 8502 machine was used for the uniaxial compression test. MoS_2 lubrication has significantly reduced the friction effect. The processing map was derived using a constitutive equation based on the hot compression test data. The strain hardening behavior of the specimens was also calculated using the Kock-Mecking method. Finally, hot compression pressure's effect on microstructure evolution and dynamic globularization has been investigated. The microstructure of the specimens was examined using conventional metallographic techniques such as optical microscopy (Olympus B 95) and scanning electron microscopy (TESCAN VEGA 3). Microstructure features were

observed using the Kroll etchant (2% HF + 6% HNO_3 + H_2O). Finally, using Clemex software, the microstructure was quantitatively analyzed.

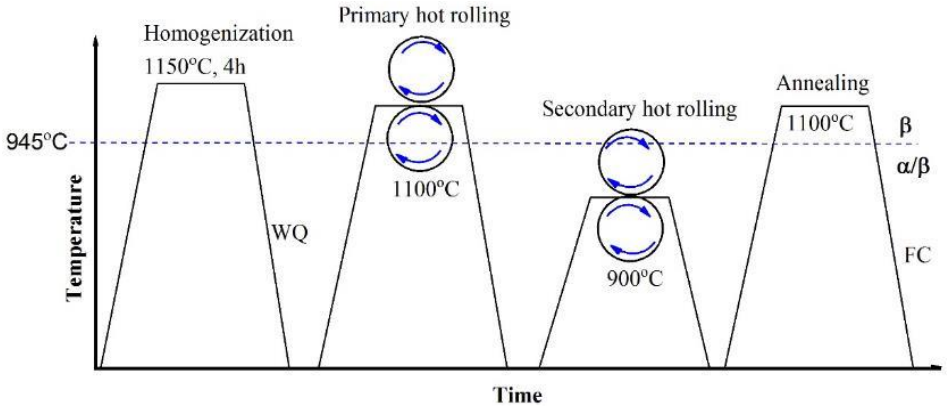

Fig. 1. The schematic illustration of thermomechanical route for achieving fully lamellar microstructure.

Results and Discussion

The fully lamellar microstructure resulting from the thermomechanical operation of Figure 1 is shown in Figure 2. the quantitative analysis of the microstructure revealed that the average thickness of the alpha is 9 ± 0.2 µm.

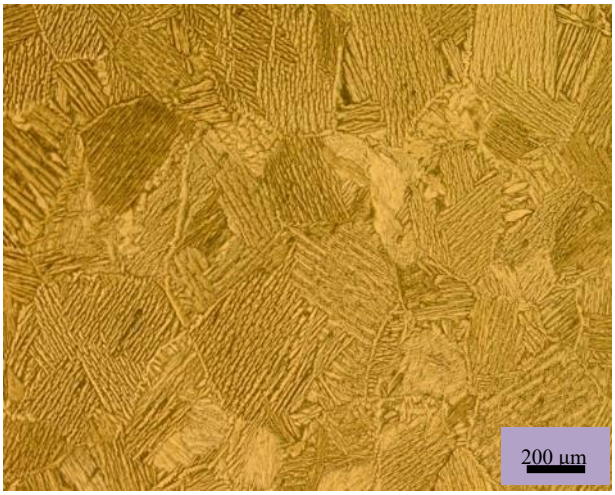

Fig. 2. Initial microstructure after primary and secondary hot rolling and heat treatment.

The effect of hot compression temperature and strain rate on the alloy's deformation behavior has been thoroughly investigated in the following sections. Figure 3 and Figure 4 show the flow curves of the alloy at single β and α+β regions, respectively. The sharp strain hardening behavior has been clearly observed in all of the extracted

stress-strain curves, which is related to the high dislocation multiplication rate via plastic deformation [14]. After applying 0.06% plastic strain, the flow stress dropped abruptly for all strain rates. The flow softening phenomenon is activated when deformation occurs at a lower temperature and a higher strain rate. The main mechanism of flow softening is related to microstructure evolution and adiabatic heat. According to the *Chav et al.* [15] declaration, the generation of heat of deformation via hot compression testing of + titanium alloys results in deformation localization and plastic deformation instability.

According to the flow curves obtained, strain hardening is balanced with the phenomenon of flow softening at higher temperatures and lower strain rates. A similar finding was reported in a previous study [16]. Because of the small amount of α phase, the occurrence of the initial stress peak phenomenon is possible. As a hard phase, the α phase is important in trapping dislocations. As a result of the rapid production and proliferation of dislocations in the early stages of deformation, stress rises rapidly. As the tension increases, however, the dislocations begin to slip from the trapped areas. Following that, the stress decreases as a peak [17].

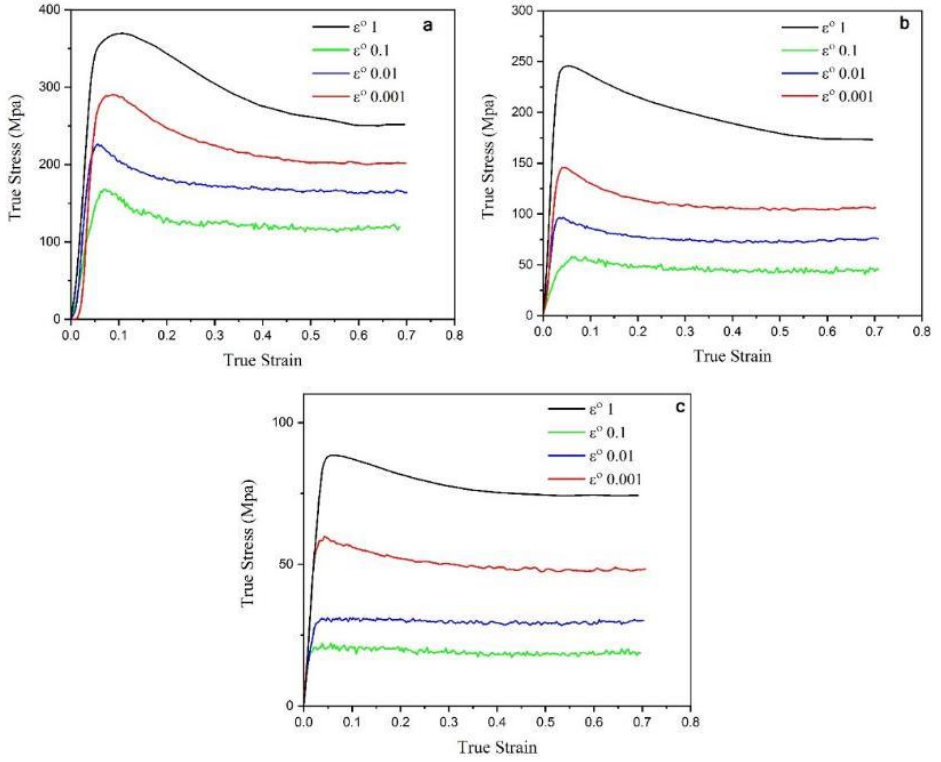

Fig. 3. Stress vs strain curve of the studied alloy at various deformation condition (i.e., strain rate and temperature): (a) 700℃ (b) 800℃ and (c) 900℃.

For all low temperatures (i.e., 700, 800, 900 °C) and low strain rates (i.e., 0.001, 0.01 s^{-1}) the stress vs strain curves has been serrated. This phenomenon has been related to a sudden increase in dislocation density and counteracting the dislocation with the same sign. The flow curve serration has been extensively reported in bcc titanium alloys [18]. *Filipart and Rock* [19] declared that the main reason for the flow stress drop is related to the alloy's chemical composition. It was reported that increasing in interstitial atoms leads to high peak stress value. In the studied alloy, the flow curve serration has been occurred for all temperatures at lower temperatures which is related to the chemical composition and dynamic recovery via hot deformation.

Kinetic analysis of hot deformation process

In this section, the relationship between flow stress, strain, strain rate, and the temperature has been established by constitutive equations. In the case of low deformation stress, the flow stress and strain are following the power law equation (E.q. 2). By increasing the stress value, the exponential law equation is dominant (E.q. 2). For all applied stress, the Arrhenius equation has been derived (E.q. 3) as per following [20]:

$$\dot{\varepsilon} = A\sigma^{n_1} \quad (1)$$

$$\dot{\varepsilon} = A_2 exp(\beta\sigma) \quad (2)$$

$$\dot{\varepsilon} = A_3[sinh(\alpha\sigma)]^n exp(-Q/RT) \quad (3)$$

The logarithmic form of the Equation 1-3 is as per following:

$$ln\dot{\varepsilon} = lnA_1 + n_1 ln\sigma \quad (4)$$

$$ln\dot{\varepsilon} = lnA_2 + \beta\sigma \quad (5)$$

$$ln\dot{\varepsilon} = lnA_3 + nln[sinh(\alpha\sigma)] - \frac{Q}{RT} \quad (6)$$

Where, A: refers to structure factor and material constant, n_1 and n_2: refer to stress index

σ: parameter of stress level, $\dot{\varepsilon}$: strain rate of deformation, R: standard molar gas constant (8.314 J/mol), T: thermodynamic temperature (K), β: material constant, α: equals to ratio β/n_1, Q: refers to the deformation activation energy, The value of n1 and β are obtained by computing the slope of $\ln(\varepsilon^{\circ}) - \ln\sigma$, $\ln(\varepsilon^{\circ}) - \sigma$ plots, respectively (figure 5). Then, according to the n_1 and β values, the α parameter is calculated.

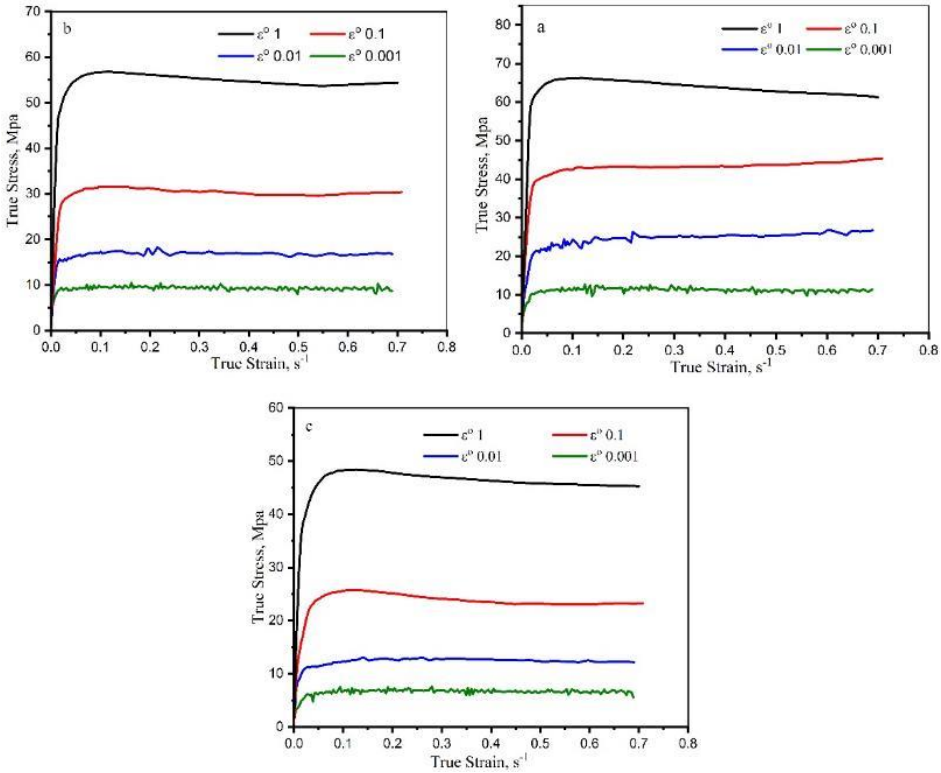

Fig. 4. True Stress-True Strain Curve of ATI425 titanium alloy at different strain rates and temperatures: (a) 970℃ (b) 1020℃ (c) 1100℃.

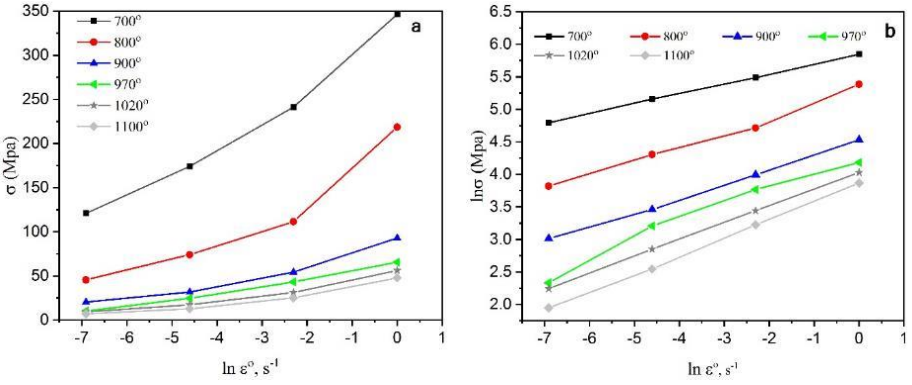

Fig. 5. Plot of (a) σ-lnε˚ (b) lnσ-lnε˚.

The amount of activation energy is obtained from Equation 7 using the slope of the Lnsinh(ασ)-Lnε˚ and Lnsinh(ασ)-1000/T diagrams of Figure 6 . The Zener-holmann parameter shows the relationship between strain rate and temperature during the hot deformation, which is calculated using Equation 8, and the Lnsinh(ασ)-LnZ variations are shown in Figure 7. From the slope and width of the origin of the Lnsinh(ασ)-LnZ curve, the stress constant (n) and material constant (LnA) parameters can be obtained, respectively. The values of α, n, Q, and LnA of ATI425 alloy for initial lamellar microstructures are presented in Table 1.

$$Q = R\left\{\frac{\partial ln\dot{\varepsilon}}{\partial ln[sinh\ (\alpha\sigma)]}\right\}T\left\{\frac{\partial ln[sinh\ (\alpha\sigma)]}{\partial(^1/_T)}\right\} \qquad 7$$

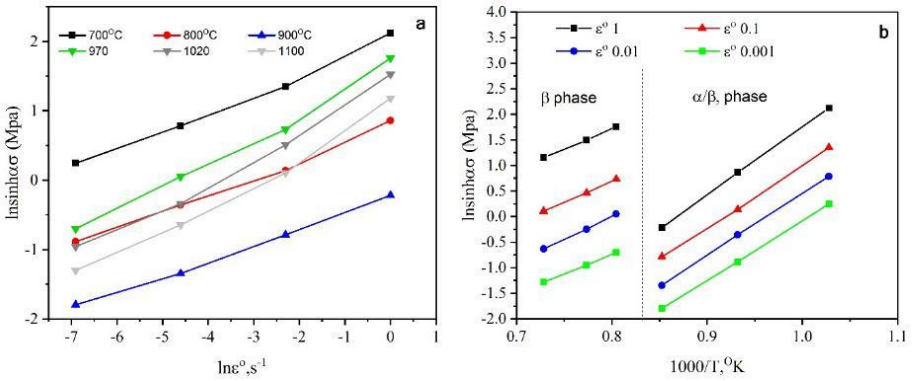

Fig. 6. Plot of lnsinh (ασ)-lnε˚-nhlnsinh (ασ)-1000/T.

Through Zener-Hollomon parameter Z, the relationship between strain rate and temperature during hot deformation can be expressed by the following formula. The extracted parameters for single β and α/β regions have been summarized in table 2. The result revealed that the value of activation energy has been significantly decreased in the β region in comparison with the α/β region.

$$Z = \dot{\varepsilon}exp\left(\frac{Q}{RT}\right) \qquad 8$$

$$Z = A_3[sinh(\alpha\sigma)]^n \qquad 9$$

$$lnZ = lnA_3 + n[lnsinh(\alpha\sigma)] \qquad 10$$

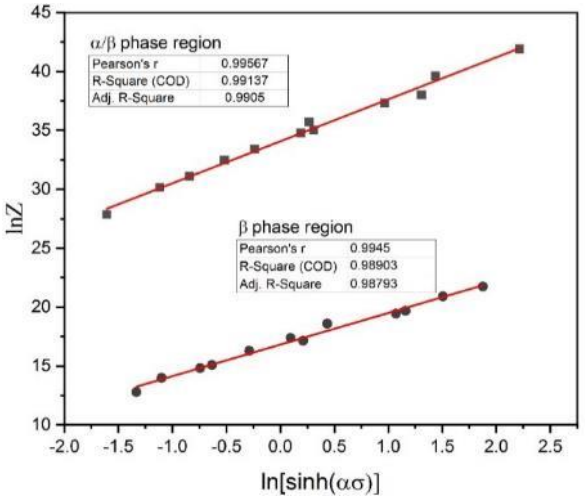

Fig. 7. Plot of the Zener–Hollomon parameter as a function of flow stress

Table 1. Values of β, n1, α, Q of ATI425 alloy.

	β	n_1	α=β/ n_1	n	Q(KJ/molºK)
α/β phase region	0.045	5.047	0.0099	3.54	348.96
β phase region	0.145	3.73	0.0033	2.75	201.79

According to table 1, it was revealed that the value of activation energy for ATI 425 alloy with starting lamellar microstructure is greater than the lattice self-Diffusion energy of α-Ti (169KJ/mol) β-Ti (153KJ/mol). The previous studies [21, 22] indicated that the activation energy of the single-phase metals with predominant dynamic recrystallization (i.e., Austenitic steel) is much more than the metals with dynamic recovery as the main microstructure evolution mechanism (Ferrite steel). Therefore, some researchers [23, 24] have tried to relate the high activation value of the two-phase titanium alloy to dynamic recrystallization mechanism. While, *Jonas et al.* [25] demonstrated that the variation in activation energy has been related to the difference of flow stress between hard (i.e., α phase) and soft (i.e., β phase) phases and also their volume fraction based on deformation temperature. In another study [26], the main reason for high activation energy in comparison with self-diffusion reaction is attributed to the α lamellas fragmentation and globularization of lamellar structure. The relationship between flow stress, deformation temperature, and strain rate of the ATI 425 alloy with initial lamellar microstructure in α/β and β regions have been established in equation 11 and equation 12, respectively.

$$\dot{\varepsilon} = 8.36 \times 10^{18}[lnsinh(\alpha\sigma)]^{2.54} exp(-348960/RT) \qquad 11$$

$$\dot{\varepsilon} = 4481125[lnsinh(\alpha\sigma)]^{2.75} exp(-201792/RT) \qquad 12$$

Processing map

A processing map is a method for controlling microstructure evolution through thermomechanical routes. As a result, after determining the engineering alloy's processing map, it is possible to optimize its deformation parameters. The alloy processing map was created by modifying the dynamic material model (DMM). *Parasad et al.* [27] were pioneers in the development of DMM. The response of material via large plastic strain has been determined in this model. The total absorbed power (P) of the alloy during hot deformation is divided into two parts as follows: 1) the energy consumed by the alloy via hot working (G) and 2) the energy consumed for microstructure promotion (J). As a result, the net value of energy is calculated using equation 13:

$$P = G + J = \int_0^{\dot{\varepsilon}} \sigma d\dot{\varepsilon} + \int_0^{\sigma} \dot{\varepsilon}\, d\sigma \qquad 13$$

The strain rate sensitivity (m) is considered to be the distribution coefficient between J and G [28, 29] which is defined according to E.q. 14:

$$m = \frac{dJ}{dG} = \left[\frac{\partial(ln\sigma)}{\partial(ln\ \dot{\varepsilon})}\right]_{T,\varepsilon} \qquad 14$$

regarding certain temperature and applied strain, the value of J can be calculated based on equation 15:

$$J = \int_0^{\sigma} \dot{\varepsilon}\, d\sigma \xrightarrow{\sigma = K\dot{\varepsilon}^m} J = \dot{\varepsilon}\sigma \frac{m}{m+1} \qquad 15$$

In an ideal state the value of m equals to 1; therefore, for an ideal linear dissipative state, the maximum energy which is required for microstructure evolution is (E.q. 16):

$$J_{max} = \frac{\sigma\dot{\varepsilon}}{2} \qquad 16$$

In the case of nonlinear state, the coefficient efficiency of power dissipation (η) is defined as per following (E.q. 17):

$$\eta = \frac{J}{J_{max}} = \frac{\dot{\varepsilon}\sigma\frac{m}{m+1}}{\frac{\sigma\dot{\varepsilon}}{2}} = \frac{2m}{m+1} \qquad 17$$

The η parameter was depicted to clarify the relationship between energy consumed via microstructure promotion and the total energy of hot the deformation process. Hence, the processing map is divided into instability and efficiency vicinity. Based on the maximum principal strain, the probability of occurrence of the instability is augmented by increasing in the efficiency of power dissipation (η). For the first time, the instability criterion has been proposed by Parasad [28] as per following (E.q. 18):

$$\xi(\dot{\varepsilon}) = \frac{\partial ln(\frac{m}{m+1})}{\partial ln\,(\dot{\varepsilon})} + m < 0 \qquad 18$$

A Two-dimension section of the derived processing map has been illustrated in fugure 8. the applied strain value of this section is 0.5. Then, according to the mentioned formulas, the cofficient efficiency of power dissipation was calculated for each state of

temperature and strain rate. Also, the instability zone has been distinguished from stability vicinity by hatching it. The extracted processing map revealed that increasing in temperature and decreasing strain rate leads to greater efficiency coffiecient. Also, increasing in applied strain resulted in wide instability vicinity. The superior work hardening condition has been recognized by a large value of η. The hot working response of the studied alloy has been defined according to the processing map. For this purpose, the extracted figure has been classified into three distinct as per following:

Region A: this region is suitable for hor deformation because the coefficient of power dissipation in this area is large than 40%. This condition has been observed for both single beta and alpha/beta phase (i.e., Temperature: 950-1100°C) and strain rate: 0.001-0.01 s^{-1}.

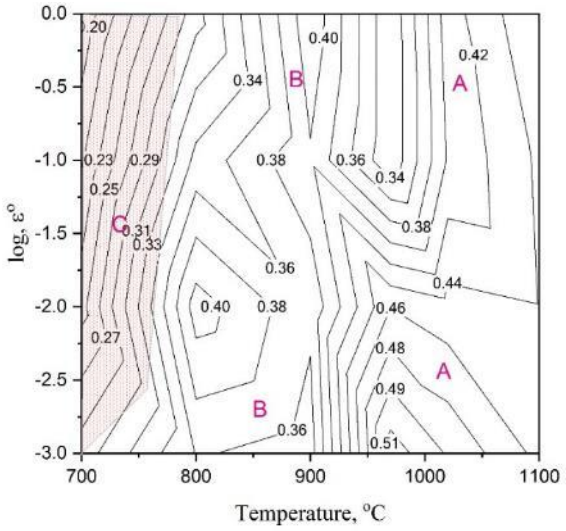

Fig.8. Derived processing map for studied alloy (applied strain = 0.5).

Region B: Hot deformation capability of this region is lower than region A. The coefficient of power dissipation in this vicinity is virtually in the range of 30-40 %. Therefore, this region has a medium capacity for hot working. In the case of the single beta phase, the medium capacity is observed when the temperature and strain rate are in the range of 950-1000°C and 0.1-1 s^{-1}, respectively. Also, in the case of the alpha/beta region, the medium capacity has been observed in the range of 800-900°C and 0.001-0.01 s^{-1}.

Region C: this vicinity has inappropriate capacity for hot working because the coefficient of power dissipation is approximately less than 25%. The instability area was observed when the temperature and strain rate is 700-800°C and 1-0.1 s^{-1}, respectively.

The formation of the shear band via hot compression at 700 °C and strain rate of 1 s^{-1} was obviously observed. It can be declared that the instability mechanism is predominantly related to strain localization.

The microstructure evolution of ATI 425 alloy via hot deformation

The microstructure evolution on α/β region

It was previously declared [30] that the microstructure evolution in titanium alloy via deformation process is directly related to the crystal orientation. The angle between the c-axis of the α crystals and the load axis is one of the major criteria for microstructure promotion. if the angle between the c axis and load axis is less than 10°, has been nominated as a hard crystal, in the case of hard orientation, the Schmidt factor value of the basal plane is near to zero. Therefore, negligible shear stress has been generated on active slips systems and dislocations have difficulty moved. Consequently, dynamic spheroidization was retarded. In the case of soft orientation, the angle between the c-axis of the α crystals and the loading axis is between the 10°-75°, the maximum shear stress has been generated in the basal planes therefore, dislocation motion is facilitated. Consequently, the dynamic recrystallization has been augmented in this vicinity.

The crystal orientation in titanium alloys is significantly related to the deformation temperature, deformation mode, and strain rate. Therefore, various volume fractions of the hard and soft α crystals have been promoted by changing the hot compression temperature and strain rate In figure 9, the microstructure of the ATI 425 alloy after hot compression test at different temperature and strain rates have been shown.

As it can be seen in figure 9.a, the spheroidization has not been occurred when the compression test was carried out at the temperature of 700 °C, strain rate of 0.001 s^{-1}. The first trace of the spheroidization has been observed when the hot compression temperature and strain rate were 700°C and 0.01 s^{-1} (figure 9.b). In this state, by proceeding with the plastic strain, the bending of α lamellar has partially appeared. By increasing the temperature from 700°C to 800°C, the bent lamellar are fragmented (figure 9. c and figure 9. d). According to the microstructure examination, it was observed that the lamellar is rotated in such a way that the rotation axis was perpendicular to the applied load axis. In the case of low and moderate strain rates (0.001-0.1 s^{-1}), similar result about the microstructure evolution in two- phase titanium alloy has been reported by *Park et al.* [7]. When the strain rate is 1 s^{-1}, the microstructure evolution mechanism is considerably different. *Motyka et al.* [31], *Voa et al.* [32] and *Margin et al.* [33] demonstrated that during the got deformation of two-phase titanium alloy with initial lamellar microstructure, high angle grain boundaries of α/α have been promoted. By increasing the applied strain, the plastic strain is localized and the lamellar structures were fragmented in the shear band vicinity.

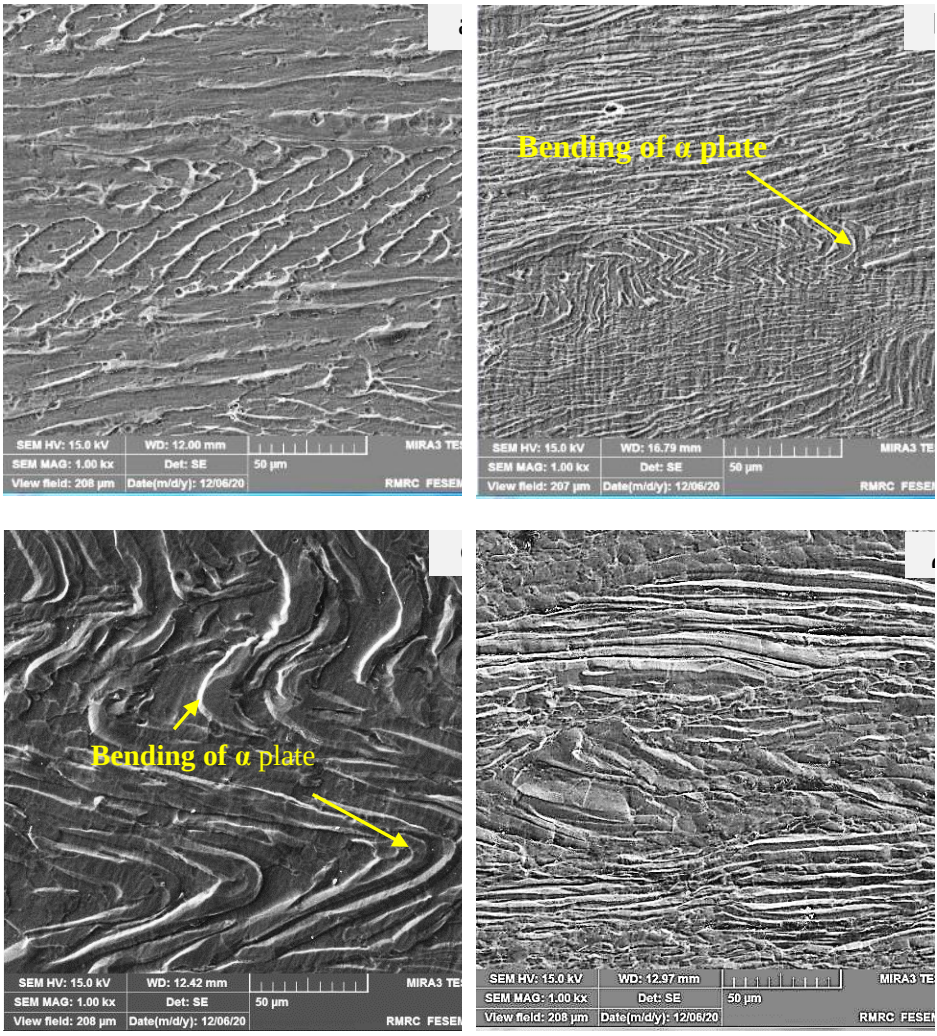

Fig. 9. Microstructure evolution of ATI425 alloy at various conditions in alpha/beta region: (a) 700°C and strain rate 0.001s^{-1}, (b) 700°C strain rate 0.01s^{-1} and (c) 800°C strain rate 0.1s^{-1}(c) 800°C strain rate 1s^{-1}.

The microstructure evolution on single β phase

The resultant microstructure of The ATI 425 alloy via hot compression test is directly related to the competition between the strain hardening and dynamic flow softening which simultaneously occurred. The main source for flow softening is regarded to be 1) heat of deformation, 2) microstructure instability which originated from dynamic recovery, dynamic recrystallization, and texture development. Dynamic recovery and dynamic recrystallization have been considered the predominant mechanisms for flow softening of the α/β titanium alloys via single β deformation [28].

The dependence of the resultant microstructure of ATI 425 ally on strain rate of temperatures via hot compression test was clearly observed in figure 10. For all strain rates and temperature, the volume fraction of the recrystallized microstructure is low. The preference sites for the nucleation of the β grains is the interface of the β/β grain boundaries (figure 10. a). However, the volume fraction of the new recrystallized β grains is low. In the case of Ti6Al4V alloy, the volume fraction of the recrystallized β grains via hot deformation at a single β region was measured to be less than 15 % [34]. *Yang et al.* [29] reported a similar result about the low volume fraction of the recrystallized β grains of ATI 425 alloy via hot deformation at a single β region. Similar result for other temperature and strain rates have been observed in figure 10.b – figure 10.f.

In the following, according to the microstructure evaluation (figure 10), the effect of temperature and strain rate on the resultant microstructure and recrystallized grains were investigated. In the case of temperature, it was clearly observed that by increasing the deformation temperature from 970°C (figure 10.a – figure 10.c) to 1100°C (figure 10.d – figure 10.f), for all strain rates (i.e., 0.001, 0.01 and 1 s^{-1}) the volume fraction of the recrystallized titanium alloy was increased. Similar result about the effect of temperature on the volume fraction of the recrystallized grains of ti64 alloy has been reported by *Ding et al.* [35].

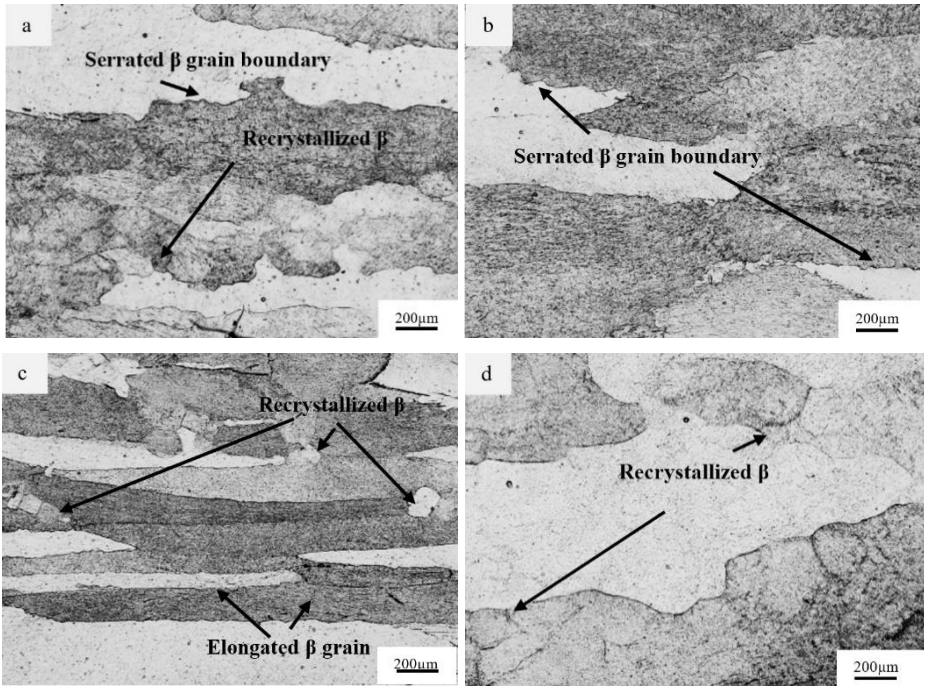

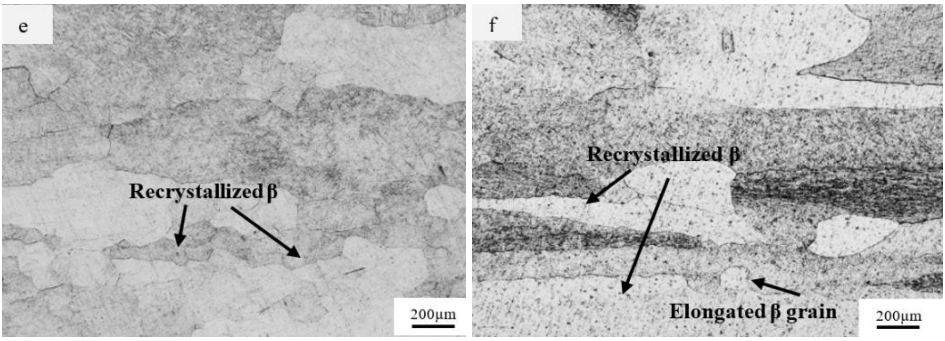

Fig. 10. Microstructure evolution of ATI425 alloy at various conditions in beta region: (a) 700°C and strain rate 0.001s^{-1}, (b) 700°C strain rate 0.01s^{-1} and (c) 800°C strain rate 0.1s^{-1}(c) 800°C strain rate 1s^{-1}.

In the case of strain rate, it was observed that by increasing the strain rate of the hot compression test from low (i.e., 0.001) to moderate (i.e., 0.01) values, the volume fraction of the recrystallized grains has been decreased. While, by reaching the strain rate to high value (i.e., 1), the recrystallization phenomenon is intensified. The microstructure examination revealed that for strain rates and temperatures, the initial β grains have been serrated which is attributed to the grain boundary migration [36].

Conclusion

The hot deformation behavior of ATI425 two-phase alloy with initial lamellar microstructure has been determined using compression test in the temperature range 700-1100°C and strain rates 0.001-1s^{-1}. The obtained results have been summarized as per following:

1. Deformation temperature and strain rate noticeably influence the resultant microstructure of ATI 425 alloy via hot compression test. In α/β region the microstructure evolution has occurred as a result of dynamic spheroidization while at β region, the dynamic recovery and dynamic recrystallization are the active mechanisms of microstructure evolution.
2. As a result of dynamic recovery, elongated β grains accompanied by serrated grain boundaries have been observed via a hot compression test at the α/β region.
3. For low and moderate strain rates (i.e., 0.001-0.1 s^{-1}), the microstructure evolution has occurred as a result of bending and fragmentation of α lamellar. While by increasing the strain rate to 1 s^{-1}, the localized shear stress is the main mechanism of globularization.
4. During the hot compression test at the α/β region, the flow stress was abruptly dropped which is associated with microstructure evolution by α lamellar fragmentation phenomenon.
5. According to the constitutive equation, the activation energy of the hot compression test in single β and α/β regions was computed. The result revealed that the value of Q for β and α/β region are 201 Kj/mol and 348 Kj/mol, respectively. Therefore, the deformation resistance of The ATI 425 alloy at α/β region is much more than β region.

6. According to the processing map of ATI 425 alloy, it was revealed that the workability capacity of the alloy is divided into three distinct vicinities. For the region with 0-25 % efficiency power dissipation, the alloy exhibits poor workability capacity. While the moderate and excellent workability of the ATI 425 alloy is related to the vicinities with 30-40 % and 40-100% efficiency power dissipation, respectively.

References

[1] D. Bryan: Mater. Sci. Forum, 786 (2014) 543-548.
[2] M. Xiong, W. Zeng, F.Tian, Y. Zhou: Mater. Sci. Eng. A, 548 (2012) 6–11.
[3] H. Margolin, P. Cohen, 1st edition, Springer, New York, 1980, 2991-2997.
[4] T. Seshacharyulu, S.C. Medeiros, W.G. Frazier, Y.V.R.K. Prasad: Mater. Sci. Eng. A, 325 (2002) 112-125.
[5] S. L. Semiatin, V. Seetharaman and I. Weiss: Mater. Sci. Eng. A, 263 (1999) 257-271.
[6] I. Weiss, G.E. Welsch, F.H. Froes, D. Eylon, in: G. Luetjering, U. Zwicker, W. Bunk (Eds.), Titanium: science and technology (1985) 1503-1510.
[7] C. H. Park, K. T. Park, D. H. Shin and C. S. Lee: Mater Trans, 49 (2008) 2196-2200
[8] R.N. Wang, Z.P. Xi, Y.Q. Zhao, Y.L. Qi: Rare Metall Mater Eng, 37 (2008) 1356-1359.
[9] Y.F. Han, W. D. Zeng, Y.L. Qi, Y. Q. Zhao: Mater. Sci. Eng. A, 528 (2011) 8410-8416.
[10] Z. C. Sun, H. Yang, Z.Tang: Comput Mater Sci, 50 (2010) 308–318.
[11] R. Ding, Z. X. Guo, A.Wilson: Mater. Sci. Eng. A, 327 (2002) 233–245.
[12] P.Wanjara, M. Jahazi, H. Monajat, S. Yue: Mater Sci Eng. A, 416 (2006) 300–311.
[13] Y. Gong: Applied Mechanics and Mater, 274 (2013) 427-431.
[14] P. M. Souza, H. Beladi, R.Singhc, B. Rolfe, P. D. Hodgson: Mater. Sci. Eng. A, 648 (2015) 265–273.
[15] Q. Chao, P. D. Hodgson, and H. Beladi: Metall. and Mater.Trans. A, 45 (2004) 2659-2671.
[16] X. Yang, H. Guo, Z. Yao and S. Yuan: High Temp. Mater. Process 2017.
[17] D. Yuan, L. Ping, X. Ke-min, Z. Qing, W. Xiao-xi: Trans. Nonferrous Metall. Soc. China, 17 (2007) 1199-1204.
[18] P. Wanjara, M. Jahazia, H. Monajatib, S. Yueb, J. P. Immarigeon: Mater. Sci. Eng. A, 396 (2005) 50–60.
[19] I. Philippart, H.J. Rack, Mat.Sci. Eng. A, 243 (1998) 196–200.
[20] Hailin Xu, Hongbo Dong and Yong Wang: Applied Mechanics and Mater, 447 (2014) 117-121.
[21] J. Jonas, C. Sellars, and W. M. Tegart: Metall. Reviews, 14 (1969)1-24.
[22] C. Roucoules, P. D. Hodgson, S. Yue, and J .J. Jonas: Metall. and Mater.Trans. A, 25 (1992) 389-400.
[23] B. Liu, Y. P. Li, H. Matsumoto, Y. B. Liu, Y. Liu, and A. Chiba: Mater. Sci. Eng A, 528 (2011) 2345-2352.
[24] H. C. Braga, R. Barbosa, and J. Breme: Scripta Met. et Materialia, 28 (1993) 979-983.
[25] L. Briottet, J. J. Jonas, and F. Montheillet: Acta Met, 44 (1996) 1665-1672.

[26] F. Pilehva, A. Zarei-Hanzaki, M .Ghambari, and H. R. Abedi: Mat. & Design, 51 (2013) 457-465.
[27] Y.V.R.K. Prasad, H.L. Gegel, S.M. Doraivelu, J.S. Malas, J.T. Morgan, K.A. Lark, and D.R. Barker: Metall. Trans. A, 15 (1984) 1883–1892.
[28] D. Zhou, W. Zeng, J. Xu, W. Chen, S. Wang: Advanced Eng. Mater, 23 (2019) 181-193.
[29] Q. Yadong, M. Wang, L. Lei, H. Xu, L. Wang, J. Qin, W. Lu , D. Zhang: Mater. Sci. Eng. A, 555 (2012) 99–105.
[30] T.R. Bieler and S.L. Semiatin: Int. J. Plasticity, 18 (2002) 1165–1189.
[31] M. Motyka, J. Sieniawski, W. Ziaja, M. Mroczka, M. B.ski: Int. Journal of Mater. Research, 5 (2018) 57-63.
[32] W. Cheng-bao, Y. He, F. Xiao-guang, S. Zhi-chao: Trans. Nonferrous Met. Soc. China, 21 (2011) 1963-1969.
[33] H. Margolin and P. Cohen: in Titanium ‘80: Science and Technology, H. Kimura and O. Izumi, eds., TMS, Warrendale, PA, 1980, 1555–61.
[34] S.L. Semiatin: Metall. Mater. Trans. A, 29 (2020) 17-29.
[35] R. Ding, Z. X. Guo, A. Wilson: Mater. Sci. Eng. A, 327 (2) 2002 233–45.
[36] P. Vo, "Flow and microstructure development of a near-alpha titanium alloy during thermomechanical processing," Phd thesis, Materials Science, 2009.